Advection, dispersion, and filtration of fine particles within emergent vegetation of the Florida Everglades

Yong H. Huang,[1,2] James E. Saiers,[1] Judson W. Harvey,[3] Gregory B. Noe,[3] and Steven Mylon[4]

Received 21 June 2007; revised 2 November 2007; accepted 4 January 2008; published 5 April 2008.

[1] The movement of particulate matter within wetland surface waters affects nutrient cycling, contaminant mobility, and the evolution of the wetland landscape. Despite the importance of particle transport in influencing wetland form and function, there are few data sets that illuminate, in a quantitative way, the transport behavior of particulate matter within surface waters containing emergent vegetation. We report observations from experiments on the transport of 1 μm latex microspheres at a wetland field site located in Water Conservation Area 3A of the Florida Everglades. The experiments involved line source injections of particles inside two 4.8-m-long surface water flumes constructed within a transition zone between an *Eleocharis* slough and *Cladium jamaicense* ridge and within a *Cladium jamaicense* ridge. We compared the measurements of particle transport to calculations of two-dimensional advection-dispersion model that accounted for a linear increase in water velocities with elevation above the ground surface. The results of this analysis revealed that particle spreading by longitudinal and vertical dispersion was substantially greater in the ridge than within the transition zone and that particle capture by aquatic vegetation lowered surface water particle concentrations and, at least for the timescale of our experiments, could be represented as an irreversible, first-order kinetics process. We found generally good agreement between our field-based estimates of particle dispersion and water velocity and estimates determined from published theory, suggesting that the advective-dispersive transport of particulate matter within complex wetland environments can be approximated on the basis of measurable properties of the flow and aquatic vegetation.

Citation: Huang, Y. H., J. E. Saiers, J. W. Harvey, G. B. Noe, and S. Mylon (2008), Advection, dispersion, and filtration of fine particles within emergent vegetation of the Florida Everglades, *Water Resour. Res.*, *44*, W04408, doi:10.1029/2007WR006290.

1. Introduction

[2] The movement of waterborne particulate matter plays an important role in the form and functioning of wetland systems. Sediment transport, deposition, and resuspension affect the ecological stability of coastal marshes by regulating their surface elevation relative to sea level [*Stevenson et al.*, 1985; *Chistiansen et al.*, 2000] and contribute to the formation and maintenance of tree islands that serve as biodiversity hotspots within freshwater wetlands [*Science Coordination Team*, 2003; *Sklar and van der Valk*, 2003; *Bazante et al.*, 2006]. Particle transport is similarly important in riparian wetlands, where changes in sediment fluxes and deposition rates have been shown to alter primary productivity, nutrient cycling, and species composition [*Cavalcanti and Lockaby*, 2006]. Suspended particles are also capable of scavenging a variety of dissolved chemicals and influence wetland water quality by governing the mobility of particle-associated contaminants (e.g., metals and herbicides) and nutrients (e.g., phosphorous) [*Sansalone and Buchberger*, 1997; *Noe et al.*, 2007].

[3] Wetland vegetation influences flow velocities and complicates descriptions of particle transport. Surface water flow in coastal and freshwater wetlands can be either laminar or turbulent with velocities ranging from less than a 1 cm s^{-1} to 15 cm s^{-1} [*Leonard and Luther*, 1995; *Nepf et al.*, 1997b; *Harvey et al.*, 2005]. Horizontal velocities within plant canopies depend on the morphology and density of the vegetation, which typically vary with depth [*Leonard and Reed*, 2002; *Lightbody and Nepf*, 2006]. For example, *Neumeier and Ciavolo* [2004] reported that flow velocities within a *Spartina maritima* salt marsh increased linearly with elevation, reflecting a reduction in vegetation density with height above the bed surface. *Lightbody and Nepf* [2006] derived a relationship appropriate for predicting the velocity profile with a *Spartina alterniflora* salt marsh from depth-dependent measurements of vegetation density. Although this relationship has not been evaluated outside of this study, it may be appropriate for predicting velocity distributions in other wetland systems.

[1] School of Environmental Studies, Yale University, New Haven, Connecticut, USA.
[2] Now at Department of Biological and Agricultural Engineering, Texas A&M University, College Station, Texas, USA.
[3] U.S. Geological Survey, Reston, Virginia, USA.
[4] Department of Chemistry, Lafayette College, Easton, Pennsylvania, USA.

0043-1397/08/2007WR006290$09.00

[4] Dispersion accounts for spreading of particles (and solutes) because of spatial and temporal variations in the flow that are not accounted for by advection [*Fischer et al.*, 1979]. Dispersion reflects the contributions from several mechanisms, including bed-induced shear, mechanical dispersion, turbulent diffusion, and exchange between mobile and immobile water zones [*Nepf*, 2004]. There are few published measurements of solute or particle dispersion in wetland canopies and even fewer evaluations of models appropriate for quantifying the phenomenon [*Nepf*, 1999; *Harvey et al.*, 2005; *Lightbody and Nepf*, 2006]. The measurements and model evaluations that are available suggest that longitudinal dispersion generally exceeds vertical dispersion and that estimates of both components of dispersion can vary by several orders of magnitude depending on the properties of the flow and plant canopy [*Nepf et al.*, 1997a, 1997b; *Ackerman*, 2002; *Saiers et al.*, 2003].

[5] Waterborne particles that are transported by dispersion and advection are susceptible to removal from the water column through settling (if they are sufficiently large and dense) and deposition on the surfaces of aquatic vegetation [*Elliot*, 2000]. Sediment capture by aquatic vegetation has been shown to account for 10 to 50% of particle immobilization within tidal marshes [*Stumpf*, 1983; *Hosokawa and Horie*, 1992; *Leonard et al.*, 1995]. *Harvey et al.* [1995] found that retention of bivalve larvae on filamentous branch structures designed to mimic benthic algae (the preferred larval substrata) depended on the branching pattern and diameter of the individual branches. *Palmer et al.* [2004] measured particle interception by cylindrical collectors emplaced in a laboratory flume and reported that observed capture rates could be expressed as a function of the Reynolds Number and the ratio of particle diameter to collector diameter. While these studies have improved our understanding of particle filtration within emergent vegetation, the number of observations is insufficient to permit quantitative inferences on particle mobility within real wetland environments.

[6] Our research is aimed at advancing knowledge of suspended particle transport through wetland vegetation. In this paper, we describe the results of four particle tracer experiments conducted under controlled forced gradient conditions in the Florida Everglades. By comparing measurements made during these experiments to model calculations, we quantify the advection, dispersion, and retention of particles and determine how these processes respond to changes in depth and vegetation composition. Our findings should be useful in informing the development of a predictive framework for the fate and transport of suspended particles and particle-associated chemicals within the Everglades and in other wetland systems.

2. Site Description and Experimental Methods

[7] Twentieth century efforts aimed at draining the Everglades to control floods and accommodate agriculture and development severely compromised the health of this wetland ecosystem [*Lodge*, 2005]. Today, half the original Everglades is gone, and large tracts of the remaining ridge-and-slough landscape (consisting of sawgrass ridges, less densely vegetated sloughs, and tree islands aligned with the flow direction) are degraded [*Science Coordination Team*, 2003]. A leading hypothesis for maintenance of the ridge and slough landscape is greater retention of suspended sediment in the ridges [*National Research Council*, 2003]. Water quality has also suffered. Prior to drainage, the Everglades received very low levels of phosphorous from atmospheric deposition, but inflows from agriculture have increased the levels of this growth-limiting nutrient leading to widespread eutrophication [*Noe et al.*, 2001]. Recent measurements made by *Noe et al.* [2007] reveal that much of this phosphorous binds to micrometer-sized particles suggesting that the fate and transport of phosphorous within the Everglades is tightly linked to processes that govern the concentrations and mobility of suspended particles.

[8] We conducted the particle tracer experiments in Water Conservation Area 3A (WCA-3A) at a field site situated within a relatively well-preserved remnant of the ridge-and-slough landscape. WCA-3A is the largest of the five water conservation areas, which were created in the 1960s by impounding 3,500 km^2 of the remaining Everglades behind earthen levees and borrow canals. These surface water impoundments were designed to achieve the often competing goals of protecting nearby agricultural and urban areas against flooding, recharging the underlying Biscayne Aquifer to prevent saltwater intrusion, receiving agricultural runoff from the Everglades Agricultural Area, and storing water for irrigation and controlled release into Everglades National Park.

[9] Two surface water flumes, the slough transition flume and the ridge flume, were constructed at the field site (26°03′22″, 80°42′20″W). The slough transition flume was positioned in the transition zone between an *Eleocharis* slough and *Cladium* ridge, where the water depth equaled 0.57 m on the day of the experiments (11 November 2005). Six species of aquatic vegetation were identified within this transition zone (Figure 1). Measurements of stem diameter (d) and frontal area per unit volume (a) were made at three 0.2-m-depth intervals on all macrophytes within a 0.5 m × 0.5 m quadrat of the transition zone (Table 1). These measurements indicate that the vegetation volume fraction (ad) increased with depth and that, near middepth (z = 0.31 m), the stem density (= a/d) equaled 2,200 m^{-2}, 92 m^{-2}, 20 m^{-2}, 16 m^{-2}, 12 m^{-2}, and 8 m^{-2} for *Eleocharis elongata*, *Cladium jamaicense*, *Eleocharis cellulosa*, *Sagittaria lancifolia*, *Bacopa carolinia*, and *Panicum hemitomon*, respectively. The ridge flume was positioned at a slightly higher elevation in the adjacent ridge, where the surface water depth equaled 0.43 m. Here the stem density of *Cladium jamaicense*, the dominant macrophyte, equaled 180 m^2 (at z = 0.23 m), which was more than ten fold greater than the stem densities of the other four macrophyte species identified within the ridge (Figure 1). Depending on depth, measurements of vegetation volume fraction (ad) were 3 to 9 times greater in the ridge than in the transition zone (Table 1).

[10] The slough and ridge flumes were 4.8 m long and 1 m wide, open to the ground surface and at their upstream ends, and oriented with their long axes approximately parallel to the ambient flow direction (Figure 2). The flume walls were constructed from 0.2 cm thick PVC sheets, which were framed on steel posts and driven 0.1 m into the peat that composed the surficial soil at the site. During the construction process, care was taken not to disturb the vegetation or soil present inside the flumes. Boardwalks

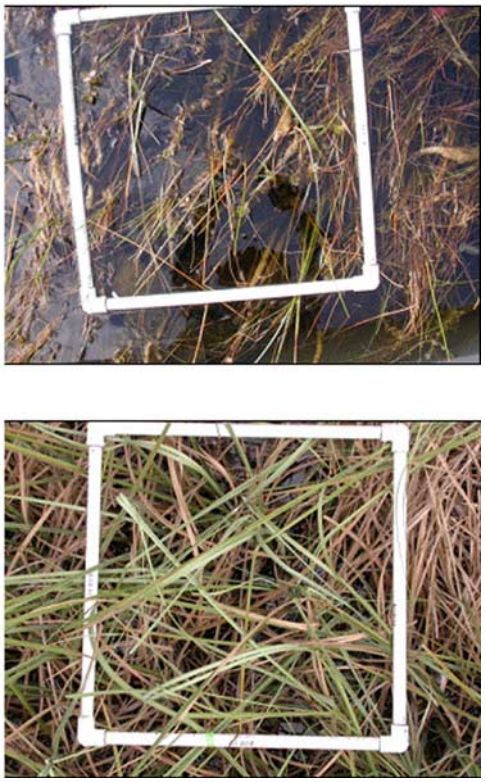

Figure 1. Vegetation of the (top) transition flume and (bottom) ridge flume. The dimensions of the white quadrant are 0.5 m × 0.5 m.

were erected along one side of each flume and between the two flumes to provide space for instrumentation and access for water sampling.

[11] Steady flow within the flumes was maintained under forced gradient conditions before, during, and after the particle injections. Two centrifugal pumps, equipped with in-line turbine flow meters, were used to withdraw surface water at a combined rate of 0.67 m^3 min^{-1} from four fully screened wells located 0.3 m inside the closed end of each flume (Figure 2). The withdrawn water was exhausted downgradient from the flume to prevent its reentry into the flume during the course of an experiment. Numerical solutions of the nonlinear diffusion equations that govern surface water flow reveal that this pumping configuration induced radial flow within 0.5 m of the withdrawal wells, but that surface water flow at greater distances from the wells was uniform and parallel with the flume walls.

[12] Red and yellow fluorescent microspheres composed of carboxylate-modified polystyrene latex were used as the particles in the tracer experiments. According to the manufacturer (Magsphere Inc., Pasadena, CA), these microspheres were 1.1 μm in diameter and slightly denser than water (1.05 g cm^{-3}) and had hydrophilic surfaces with a charge density 0.015 meg g^{-1}. Calculations made with Stokes law indicate that the settling rate of these micrometer-sized particles is less than 0.1 cm d^{-1}, and hence sedimentation did not contribute significantly to particle immobilization in the experiments. The stock suspensions of the yellow and red microspheres were diluted to a concentration of 6 g L^{-1} with filtered (0.2 μm) surface water collected from the field site prior to their application in the tracer experiments.

[13] The yellow and red fluorescent particles were introduced simultaneously at two depths in horizontal line source injections (Figure 2). In both the ridge and transition zone experiments, the yellow particles were used in the shallow injection, while the red particles were used in the deep injection (see Table 2 for injection depths). The line sources, which extended across the width of the flume and were positioned 0.3 m downstream from the flume entrance, consisted of Plexiglas tubes (2 cm diameter) with 0.1 cm holes spaced 1 cm apart. Peristaltic pumps were used to control the flow of the particle suspensions through the Plexiglas injection tubes, and preliminary experiments conducted in the laboratory showed that the particle flux was uniform over the length of the injection tube. In the field,

Table 1. Measurements of Frontal Area Per Unit Volume (a), Stem Diameter (d), and Vegetation Volume Fraction (ad) as a Function of Elevation Above the Ground Surface (z)[a]

	a, cm^{-1}			d, cm			ad		
Transition	z = 11 cm	z = 31 cm	z = 51 cm	z = 11 cm	z = 31 cm	z = 51 cm	z = 11 cm	z = 31 cm	z = 51 cm
Bacopa caroliniana	1.0×10^{-3}	4.3×10^{-4}	1.4×10^{-3}	0.36	0.36	0.36	3.6×10^{-4}	1.5×10^{-4}	5.1×10^{-4}
Cladium jamaicense	3.3×10^{-2}	8.5×10^{-3}	8.5×10^{-3}	1.04	0.92	0.76	3.5×10^{-2}	7.8×10^{-3}	6.5×10^{-3}
Eleocharis cellulosa	1.0×10^{-3}	4.7×10^{-4}	5.6×10^{-4}	0.24	0.24	0.24	2.4×10^{-4}	1.1×10^{-4}	1.3×10^{-4}
Eleocharis elongata	2.1×10^{-2}	2.2×10^{-2}	1.6×10^{-2}	0.10	0.10	0.10	2.1×10^{-3}	2.2×10^{-3}	1.5×10^{-3}
Panicum hemitomon	4.2×10^{-4}	2.5×10^{-4}	9.1×10^{-5}	0.35	0.31	0.23	1.5×10^{-4}	7.5×10^{-5}	2.1×10^{-5}
Sagittaria lancifolia	6.5×10^{-4}	6.5×10^{-4}	8.2×10^{-4}	0.41	0.41	0.41	2.7×10^{-4}	2.7×10^{-4}	3.3×10^{-4}
All species[b]	5.8×10^{-2}	3.3×10^{-2}	2.7×10^{-2}	0.13	0.11	0.11	7.3×10^{-3}	3.5×10^{-3}	3.0×10^{-3}
Ridge	z = 7 cm	z = 23 cm	z = 43 cm	z = 7 cm	z = 23 cm	z = 43 cm	z = 7 cm	z = 23 cm	z = 43 cm
Cephalanthus occidentalis	9.7×10^{-5}	0	9.3×10^{-5}	0.24		0.23	2.3×10^{-5}	0	2.1×10^{-5}
Cladium jamaicense	2.1×10^{-2}	1.6×10^{-2}	3.7×10^{-2}	1.04	0.89	0.75	2.1×10^{-2}	1.4×10^{-2}	2.8×10^{-2}
Justicia angusta	1.9×10^{-5}	6.3×10^{-5}	1.2×10^{-4}	0.30	0.02	0.08	5.8×10^{-6}	1.3×10^{-6}	9.5×10^{-6}
Panicum hemitomon	7.1×10^{-5}	8.6×10^{-4}	9.1×10^{-5}	0.35	0.31	0.23	2.5×10^{-5}	2.6×10^{-4}	2.1×10^{-5}
Utricularia foliosa	7.5×10^{-3}	0	0	0.04			3.0×10^{-4}	0	0
All species[b]	2.8×10^{-2}	1.7×10^{-2}	3.8×10^{-2}	1.00	0.71	0.72	2.8×10^{-2}	1.2×10^{-2}	2.7×10^{-2}

[a]Elevations correspond to the midpoint of the vegetation-sampling interval.
[b]All species values of a are obtained through summation over individual species, and all species values of d are stem count–weighted averages.

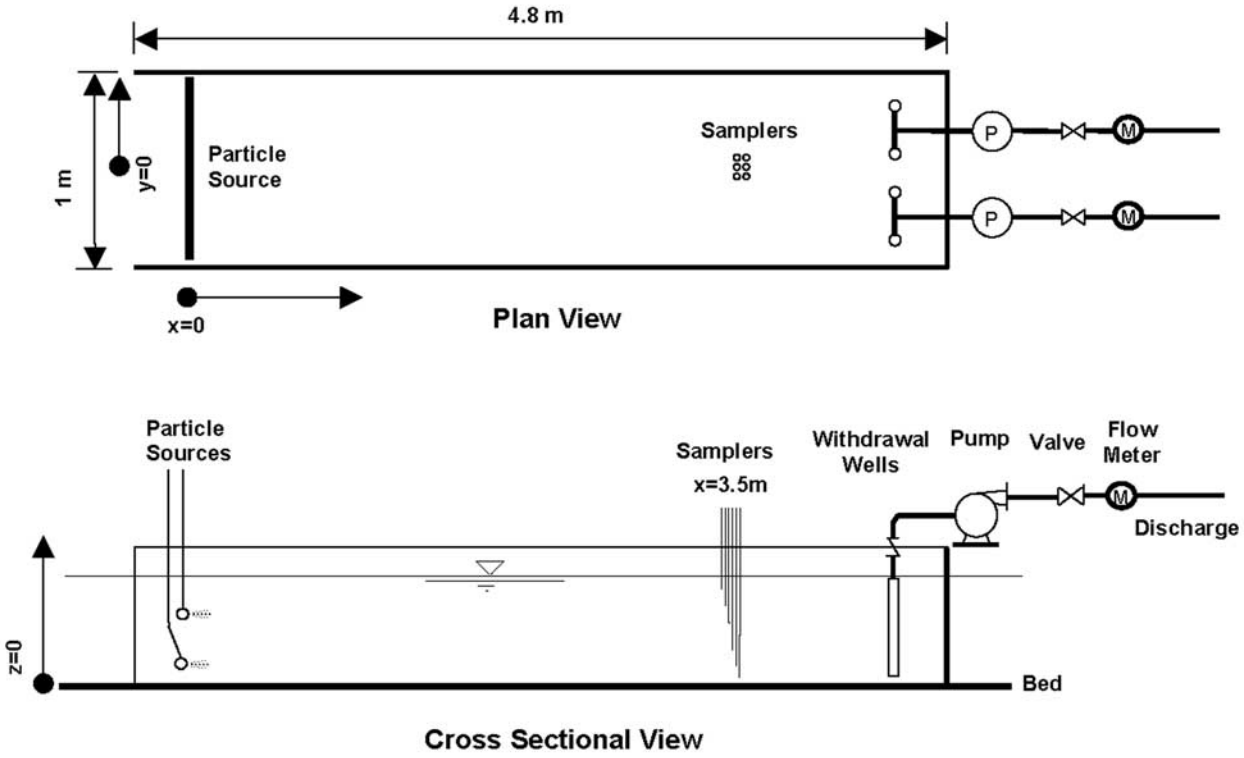

Figure 2. Positions of the tracer line sources, samplers, and water withdrawal wells used in the particle tracer experiments. The x coordinate is parallel to surface water flow and the long dimension of the flume. Elevation is measured upward from the ground surface, where $z = 0$. Water was pumped from the water withdrawal wells (at $x = 4.5$ m) and discharged outside the flumes in order to establish forced gradient conditions. Only the upgradient end of the flume is open.

the yellow and red particles were injected at a rate of 291 to 301 mL min^{-1} for a period of 28.8 to 30.0 minutes (Table 2), whereupon the peristaltic pumps were reversed to achieve an abrupt termination of the particle input pulse.

[14] Sampling for the fluorescent microspheres began before the start of the injections and continued for 1 hour after their termination. Water samples (20 mL) were repeatedly collected in glass scintillation vials by using multichannel peristaltic pumps to withdrawal water from stainless steel sampling tubes (0.3 cm diameter) installed at six different depths 3.5 m downgradient from the injection (see Table 2 for sampling depths). The sampling frequency varied from 30 seconds per sample, when concentrations were expected to change rapidly (around the times of initiation and termination of the particle injections), to 4 minutes, when particle concentrations were expected to change more gradually.

[15] The concentrations of the yellow and red microspheres were measured in the laboratory by fluorescence spectrophotometery (FluoroMax-3, HORIBA Jobin Yvon, Inc., NJ). Peak excitation/emission wavelengths of 412/480 nm and 512/570 nm were used for the yellow and red microspheres, respectively. At both 480 nm (yellow) and 570 nm (red) wavelengths, the Everglades water pro-

Table 2. Experimental Measurements

Water Depth, m	Sampler Elevation, m	Tracer	Line Source Elevation, m	Particle Injection Rate, mL min^{-1}	Injection Duration, min
			Ridge		
0.43	0.370, 0.305, 0.240, 0.175, 0.110, 0.045	Yellow Red	0.33 (shallow) 0.1 (deep)	291 301	28.8 28.8
			Transition		
0.57	0.488, 0.408, 0.328, 0.248, 0.168, 0.088	Yellow Red	0.43 (shallow) 0.15 (deep)	298 301	30.0 30.0

duced a stable background emission, which was deducted in our analysis of the calibration standards and experimental samples to isolate the emissions associated with the particles. Our tests indicated that the detection limit of the red and yellow particles was 0.05 mg L^{-1} and that the concentrations of the yellow and red particles could be resolved separately when both particles were present in the samples.

3. Mathematical Model

[16] We quantified particle advection, dispersion, and immobilization rates in the field experiments by comparing the measured breakthrough curves on particle transport to those calculated by a mathematical model. The model solves an equation appropriate for describing transport in a domain of steady and uniform water depth, where surface water flow parallels the long axis of the flume, and the flow velocity varies with depth, but not over the flume width or length:

$$\frac{\partial C}{\partial t} = -u(z)\frac{\partial C}{\partial x} + D_x\frac{\partial^2 C}{\partial x} + \frac{\partial}{\partial z}\left(D_z\frac{\partial C}{\partial z}\right) - \lambda C \qquad (1)$$

where C is the particle concentration in the surface water, t is time, z is the vertical coordinate (measured upward from the ground surface), x is the coordinate in the direction of advective transport (equal to zero at the line source), u is the surface water flow velocity (which varies with depth), D_x and D_z are the longitudinal and vertical dispersion coefficients, respectively, and λ is a rate coefficient for particle capture by aquatic vegetation.

[17] We employed a finite element method to solve equation (1) for a two-dimensional domain measuring 4.5-m long and either 0.57-m deep (transition flume) or 0.43-m deep (ridge flume). The numerical solutions were obtained for zero initial particle concentrations, zero total particle flux across the free surface and ground surface, and a zero gradient in particle concentration across the upstream and downstream ends of the model domain. A specified flux condition was used to simulate particle injection through the line sources, which were located 0.3 m inside the upstream end of the flumes. Comparison of finite element solutions for simplified boundary conditions to corresponding analytical solutions [*Domenico*, 1987] indicated that stable and accurate numerical solutions could be obtained by discretizing the domain into 5,000 elements.

4. Parameter Estimation

[18] We applied the model in inverse mode to estimate the model parameters that quantified longitudinal dispersion (D_x), vertical dispersion (D_z), and filtration (λ) in the field experiments. A Levenberg-Marquardt algorithm was used to find the values of the model parameters that minimized the sum-of-squared differences between measured and modeled particle concentrations. Separate model inversions were performed for the shallow and deep injections in the ridge and transition zone experiments.

[19] The velocity profile ($u(z)$), in addition to values of D_x, D_z, and λ, is needed to parameterize the transport model. We originally specified $u(z)$ from depth-dependent measurements of water velocity, which were made near the center of the flumes with an acoustic Doppler velocimeter (ADV) following the protocols of *Riscassi and Shaffranek* [2003]. Use of the ADV-based velocity profiles led to poor model description of the observed particle breakthrough curves. This poor model-data agreement suggests that the point estimates of velocity provided by the ADV are not appropriate for quantifying particle advection rates, which reflect an average of longitudinal water velocities that vary along the flume length. In place of the ADV-measured velocity profiles, we assumed that u increased linearly with z and calculated the slope of the u-z relationship from estimates of flow velocity made at the elevations of the yellow particle (shallow) and red particle (deep) line sources. The flow velocities at the elevations of the shallow and deep line sources were determined from average time required for the particles to travel from their respective sources to the sampling station located 3.5 m downgradient:

$$u(x, z = z_i) = {}^{3.5\mathrm{m}}\Big/_{(T_{0.5} - T_t)} \qquad (2)$$

where $u(x, z = z_i)$ is the average velocity along a horizontal streamline at z_i, the elevation of particle injection, T_t is the time in which the particle injection was terminated, and $T_{0.5}$ is time in which particle concentrations at the sampler positioned at $z \approx z_i$ declined to one half their average, steady state levels that existed to prior termination of the particle input pulse.

[20] Model-simulated particle concentrations failed to mimic measured concentrations in simulations in which D_z was assumed to be constant; therefore, for the simulations shown in this work, we relaxed the simplifying assumption of constant D_z and let this parameter vary as a function of water velocity:

$$D_z = \alpha u(z) \qquad (3)$$

where α is a proportionality constant that is estimated from model inversion.

5. Results

5.1. Ridge Experiments

[21] Model-calculated concentrations agree reasonably well with those measured at the six depths in the ridge experiments (Figures 3a and 3b). Values of R^2, a normalized measure of the goodness of model fit to the data, exceed 0.89 for both shallow injection experiment with the yellow particles and the deep-injection experiment with the red particles (Table 3). The unexplained variation is greatest for the deep-injection experiment, where the model fails to capture the slow approach toward steady state concentrations (Figure 3b). Comparatively minor discrepancies arise between computed and measured concentrations in the shallow-injection experiment, where the model fails to reproduce the spike in concentrations measured at z = 0.37 m (Figure 3a). In both cases, the model succeeds in approximating the timing of initial breakthrough, the magnitude of the steady, plateau concentrations at each depth, and the rate of decline in concentrations following cessation of the input pulse.

[22] The general agreement between modeled and measured results suggests that our assumptions regarding the

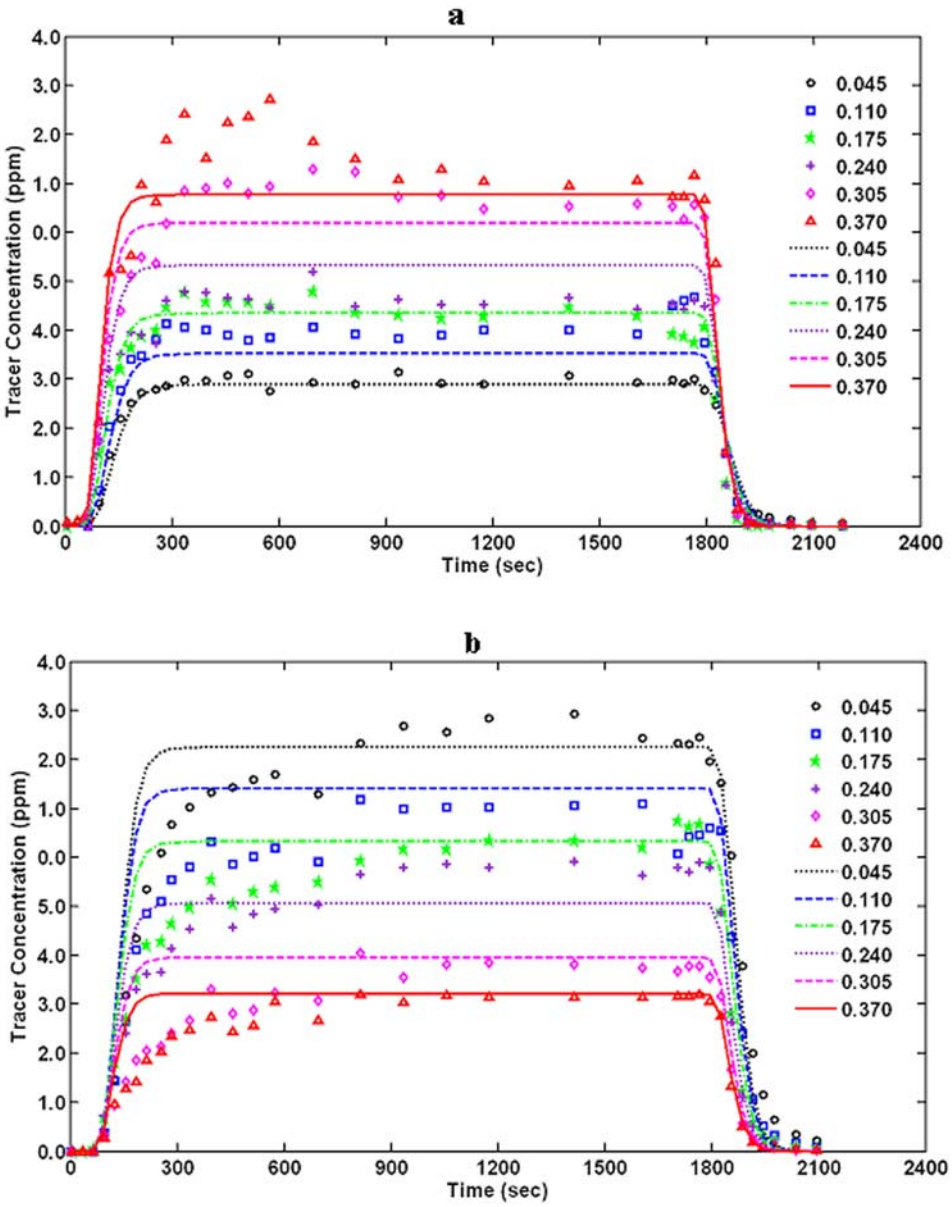

Figure 3. Model-calculated breakthrough curves (lines) and those measured in experiments conducted in the ridge flume (symbols): (a) shallow (yellow particle) injection and (b) deep (red particle) injection. The legend refers to the elevations of the samplers (in units of meters) that were located 3.5 m downgradient from the particle line sources.

Table 3. Best Fit Parameter Values and Standard Errors of the Parameter Estimates[a]

Treatment	A,[b] cm	D_x, cm^2 s^{-1}	$\lambda \times 10^{-3}$, s^{-1}	R^2
		Ridge		
Shallow injection	0.57 (0.02)	48.4 (0.8)	0.02 (0.08)	0.953
Deep injection	0.67 (0.03)	30.5 (1.8)	0.30 (0.05)	0.894
		Transition		
Shallow injection	0.092 (0.005)	0.21 (0.2)	7.25[b] (0.10)	0.926
Deep injection	0.055 (0.0014)	0.41 (0.006)	1.84[c] (0.04)	0.984

[a]The standard errors of the parameter estimates are listed in parentheses and provide a measure of the sensitivity of the model fit to changes in the parameter value [see *Press et al.*, 1989].
[b]The parameter α appears in equation (3) and relates the vertical dispersion coefficient, D_z, to the water velocity, $u(z)$.
[c]The best fit values of λ likely overestimate filtration rates in the transition zone experiments (see section 5.2).

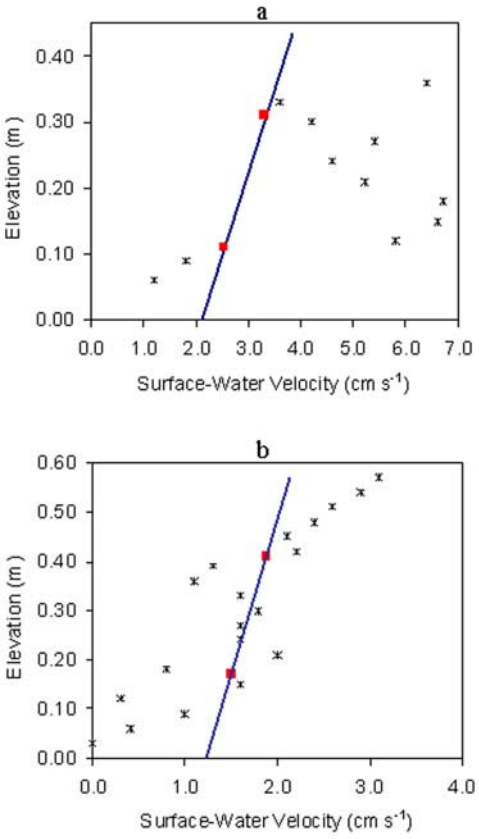

Figure 4. Vertical profiles of velocity for the (a) ridge flume and (b) transition zone flume. The asterisks denote measurements made with the acoustic Doppler velocimeter, while the red squares represent velocities estimated from the average particle travel times. The lines were obtained by linear extrapolation of velocities obtained from the particle traveltime analysis and were used to specify the velocity field in the model simulations.

velocity distribution provide a suitable representation of the flow field. Linear extrapolation of estimates made at the two particle-injection depths yields longitudinal velocities that vary from 2.1 cm s^{-1} at the ground surface to 3.8 cm s^{-1} at the water surface. Although this extrapolation overestimates the real velocity at the ground surface, which must equal zero, this misrepresentation does not seriously jeopardize the description of the measured breakthrough curves, probably because velocities increase sharply within a ≈1-cm region close to the bed, but vary more gradually over the remaining portion of the water column [*Nepf et al.*, 1997b]. The ADV measurements, on the other hand, exhibit no pronounced linear trend, but increase from 1 cm s^{-1} near the ground surface to 7 cm s^{-1} at z = 0.2 m, generally decrease between z = 0.2 and z = 0.3 m, and increase again toward the surface (Figure 4). We attribute the discrepancy between the ADV measurements and the traveltime-based velocities to differences in the scale of the estimates. The ADV measures velocity over a small volume (5 cm^3), while the traveltime-based estimates average particle velocities over the length of the flume.

[23] The longitudinal dispersion coefficient (D_x) quantifies spreading along the length of the flume induced by small-scale variations in velocity that are not accounted for by the simulated velocity field (i.e., $u(z)$). The best fit values D_x equal 48.0 cm^2 s^{-1} and 30.5 cm^2 s^{-1} for the shallow and deep injections, respectively. Estimates of D_x can be used to compute the Peclet number (Pe), a dimensionless parameter that quantifies the ratio of timescale for dispersion to the depth-dependent timescale for advection [*Tritton*, 1988]:

$$Pe = u(z)L/D_x \tag{4}$$

where L, the characteristic length, is taken as the distance between the particle injection and sampling locations. Values of Pe range from 15 to 28 and from 24 to 44 for the shallow and deep injections, respectively, indicating that advection, rather than dispersion, dominated particle transport in the ridge experiments.

[24] The vertical dispersion coefficient influences the distribution of particle concentrations over depth, with breakthrough concentrations of particles becoming more uniform over depth as D_z increases in magnitude. We assumed that vertical dispersion increases linearly with water velocity according to equation (3). The best fit values of the proportionality constant (α) that quantify this linear relationship vary by only 20% between the shallow and deep injections (Table 3), and calculations of D_z made with (3) range from 1.2 cm^2 s^{-1} to 2.5 cm^2 s^{-1} and are more than an order of magnitude less than D_x.

[25] The parameter λ quantifies the rate of irreversible particle filtration. Changes in the value of this parameter regulate the magnitude of the steady state concentrations that occur between the ascending and descending limbs of the breakthrough curves. The estimate of λ determined from the shallow-injection experiment in the ridge flume is close to zero (Table 3), indicating that the yellow particles traveled nearly conservatively through the sawgrass vegetation that dominated the ridge. Filtration rates were greater in the ridge experiment with the red particles (deep injection), and, in this case, the best fit value of λ equals 3×10^{-4} s^{-1}. This estimate corresponds to a timescale for filtration (λ^{-1}) of 0.93 hours, which is 28 times greater than the depth-averaged timescale for advection. Although our assumption of a constant filtration coefficient (λ) led to a suitable approximation of the measured breakthrough concentrations in the ridge experiments, the sensitivity of λ to particle-injection depth suggests that filtration kinetics were not truly uniform, but varied with depth owing to heterogeneity in water velocity, stem density, and stem morphology.

5.2. Transition Zone Experiments

[26] The model reproduced the principal characteristics of particle transport in the transition zone experiments, with R^2 calculations exceeding 0.92 for both the shallow and deep injections (Figures 5a and 5b and Table 3). Deviations between measured and modeled results are most apparent in the description of the breakthrough curves from the shallow-injection experiment. In this case, the model fails to simulate the spike in concentrations between 300 and 500 seconds at z = 0.41 m and underestimates the steady, plateau concentrations (between 300 and 1900 seconds) at z = 0.33 m and 0.49 m (Figure 5a).

[27] The traveltime-based estimates of $u(z)$ used in the model simulations (made through application of equation (2))

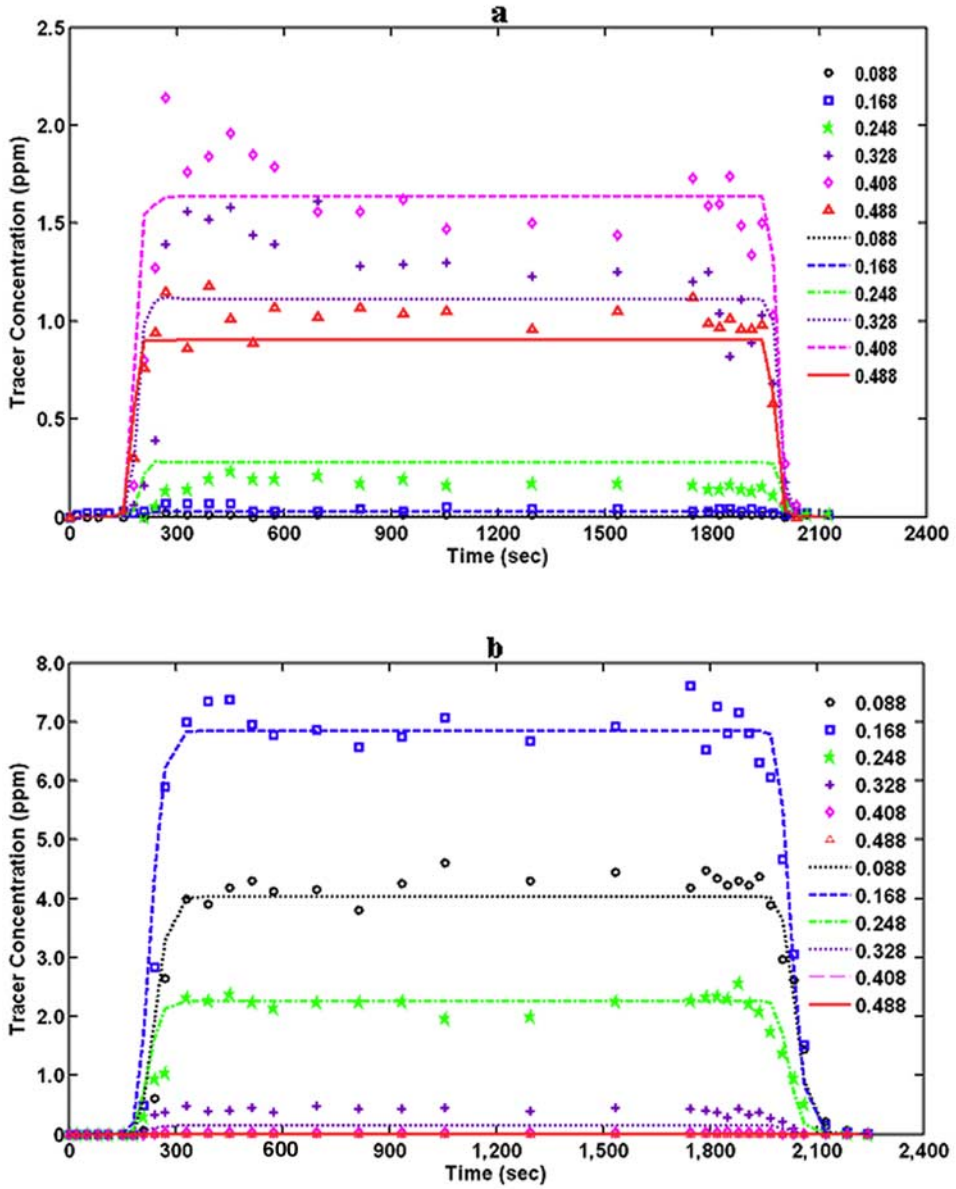

Figure 5. Model-calculated breakthrough curves (lines) and those measured in experiments conducted in the transition zone flume (symbols): (a) shallow (yellow particle) injection and (b) deep (red particle) injection. The legends refer to the elevations of the samplers (in units of meters) that were located 3.5 m downgradient from the particle line sources.

increase from 1.2 cm s^{-1} at the ground surface to 2.1 cm s^{-1} at the water surface. These estimates are generally within a factor of two of measurements made with the ADV (Figure 4). The ADV measurements increase in a linear fashion with elevation in accordance with our assumptions; however, they exhibited a greater range than our traveltime-based estimates of velocity, varying from nearly zero near the base of the water column (at z = 0.04 cm) to 3.1 cm s^{-1} at the top of the water column (Figure 4).

[28] Results of the inverse analysis demonstrate that particle dilution by longitudinal and vertical dispersion was small in the transition zone experiments. Values of D_x equal 0.41 cm^2 s^{-1} for the deep injection and 0.20 cm^2 s^{-1} for the shallow injection and are at least 74 times less than the corresponding values of D_x estimated from the ridge experiments (Table 3). The best fit estimates of α that govern the linear relationship between D_z and $u(z)$ vary by less than a factor of two between the shallow-injection and deep-injection treatments, but are more than six fold less than corresponding estimates of α from the ridge experiments. Calculations of D_z made for middepth (z = 0.29 m) equal 0.15 cm^2 s^{-1} and 0.09 cm^2 s^{-1} for the shallow- and deep-injection experiments, respectively, and indicate that the timescale for complete vertical mixing (h^2/D_z, where h is water depth) in the transition zone is between 6 and 10 hours, much greater than the 20 minutes required for complete vertical mixing in the ridge experiments.

[29] The best fit values of the particle filtration coefficient (λ) are greater than 1.8 h^{-1} for both transition zone experiments and are considerably greater than those determined

from analysis of the ridge experiments (Table 3). We believe, however, that these λ values substantially overestimate the particle filtration rates in the transition zone experiments. Particle migration could be tracked qualitatively by eye, and observations made during the transition zone experiments revealed that the microspheres traveled preferentially along one side of the flume. Owing to this preferential transport (which presumably arose from the heterogeneity in the density of the aquatic vegetation), particle concentrations varied across the flume width, with concentrations declining from the flume wall toward the middle of the flume, where the water samplers were positioned. The low concentrations in the center of the channel were incorrectly accounted for in the model inversion by high λ, when, more likely, they reflected conditions along the edge of a particle transport plume that was diluted by lateral mixing with microsphere-free water. We cannot quantify the degree to which our inverse analysis overestimates particle filtration rates, and thus we cannot exclude the possibility of negligibly small filtration rates in the transition zone experiments.

[30] Although the cross-flume variations in flow and particle concentrations led to overestimation of λ in the transition zone experiments, results of additional analyses suggest that it did not jeopardize quantification of longitudinal and vertical dispersion. We conducted simulations with a three-dimensional transport model that allowed for cross-flume variation in particle concentrations owing to lateral dispersion. These three-dimensional simulations were conducted for the case of conservative transport ($\lambda = 0$) and with various combinations of the coefficients for longitudinal dispersion (D_x), vertical dispersion (D_z), and lateral dispersion (D_y). For each simulation, breakthrough concentrations were recorded along the edge of the particle plume to represent the off-centerline sampling that we believe occurred in the transition zone experiments. When these breakthrough concentrations were used as calibration targets in inverse simulations with our two-dimensional model (i.e., equation (1)), the best fit values of λ exceeded zero, but the estimates of D_x, and D_z used in the original simulations with the three-dimensional model were recovered. On the basis of these results, we infer that application of our two-dimensional model to the transition zone experiments yielded accurate estimates of longitudinal and vertical dispersion because the effects of lateral dispersion in diluting particle concentrations were represented phenomenologically by filtration.

6. Discussion

[31] Our findings reveal that micrometer-sized latex particles can exhibit high mobility within Everglades surface waters, suggesting that similarly sized particles, such as bacteria, protozoa, colloidal organic matter, and micrometer-sized mineral precipitates may, under some conditions, be transported considerable distances within wetlands. Our analysis further reveals that this particle transport is complex, varying with depth and between ridge and transition zone environments.

6.1. Particle Advection

[32] In both the ridge and transition zone experiments, particle advection rates could be described as a linear function of elevation and were nearly two fold greater at the top of the water column than near the ground surface. *Neumeier and Ciavolo* [2004] similarly reported linear velocity profiles for surface water flow through a *Spartina maritima* salt marsh, and *Leonard and Luther* [1995] observed that water velocities increased proportionately with elevation within a *Distichlis spicata* canopy. Others studies have shown that nonuniformity in plant morphology and density lead to more complex velocity profiles [e.g., *Ackerman*, 2002; *Leonard and Reed*, 2002], including cases where relatively low velocities occur near the top of the water column within dense canopies of floating vegetation [*Harvey et al.*, 2005]. *Lightbody and Nepf* [2006] derived a relationship that expresses the vertical velocity profile in terms of vegetation frontal area (a):

$$u(z) = \sqrt{\frac{\tilde{a}}{a(z)}}\tilde{u} \tag{5}$$

where $\tilde{u}$ represents the velocity at a reference height above the bed where vegetation drag dominates and $\tilde{a}$ is the frontal area at this same height. *Lightbody and Nepf* [2006] explain that this relationship is applicable for conditions in which $ad < 0.10$ and for values of Re_d, the stem Reynolds Number ($=ud/\mu$, where μ is the dynamic viscosity), ranging from 10 to 10,000. These investigators found good agreement between calculations made with (5) and velocity profiles measured within a *Spartina alterniflora* salt marsh. Predictions of $u(z)$ made by using our measurements of a in equation (5) closely resemble the velocities determined from analysis of particle transport in the transition zone experiments (Table 4). Agreement is not as good in the ridge experiments, at least near the top of the water column, but, even here, the percent difference between empirical and theoretically determined velocities is only 60% (Table 4). These results, when taken together with those of *Lightbody and Nepf* [2006], suggest that a simple method that is parsimonious in its parameterization is suitable for estimating the velocity profile within emergent canopies.

6.2. Longitudinal Dispersion

[33] There are few published estimates of longitudinal dispersion with which to compare our measurements. Our estimates of D_x for the transition zone experiments are within a factor of 2.4 of those reported for the transport of 0.3 μm TiO_2 particles and a conservative solute (bromide) through an *Eleocharis* slough located south of our study site in Everglades National Park [*Saiers et al.*, 2003; *Harvey et al.*, 2005]. This general correspondence in D_x between studies reflects similarity in flow regimes (flow was laminar (i.e., $Re_d < 25$) at both sites) and similarity in aquatic vegetation (*Eleocharis sp.*), except near the water surface where a layer of *Utricularia purpurea* floated at Everglades National Park site, but was absent from transition zone flume. Estimates of D_x for the ridge experiments were considerably greater than for the transition zone, but of the same order of magnitude as the value of D_x reported by *Lightbody and Nepf* [2006] for the migration of Rhodamine through a *S. alterniflora* salt marsh.

[34] The difference in dispersion between the ridge and transition zone experiments can be interpreted through consideration of the mechanisms that govern particle mixing

Table 4. Values u, D_x, and D_z Determined Empirically From the Tracer Experiments and Those Determined From Published Theory[a]

	u, cm s^{-1}		D_x, cm^2 s^{-1}		D_z, cm^2 s^{-1}	
z, cm	Empirical	Theoretical	Empirical[b]	Theoretical	Empirical[c]	Theoretical
			Transition			
11	1.4	1.4	0.31	0.37	0.10	N.A.[d]
31	1.7	1.9	0.31	0.37	0.13	N.A.
51	2.0	2.0	0.31	0.40	0.15	N.A
			Ridge			
7	2.4	2.4	39.5	1.8	1.5	0.55
24	3.0	3.1	39.5	1.6	1.9	0.37
43	3.8	2.1	39.5	2.0	2.4	0.62

[a]Measurements of frontal area per unit volume (a) and stem diameter (d), which are given as a function of elevation (z) in Table 1, are used to compute the theoretical values of u, D_x, and D_z from equations (5), (6), and (7), respectively.
[b]Empirical values of D_x are computed by averaging the values of D_x from the shallow and deep injections (see Table 3).
[c]Empirical values of D_z were computed with equation (3) by using the average of the best fit values of α from the shallow and deep injections (see Table 3).
[d]Flow was laminar in the transition zone experiments and hence equation (7), which is used to compute D_z when turbulent mixing governs vertical dispersion, is not applicable (N.A.).

and the effects that variations in the properties of the flow and aquatic vegetation have on these mechanisms. Longitudinal dispersion describes particle mixing due to variations in velocities that are not accounted for by $u(z)$. These variations in velocity arise, in part, from (1) recirculation zones directly behind the stems, where the average velocity is zero, (2) wakes downstream of the recirculation zones, where the velocity is nonzero but less than the spatially average flow speed ($u(z)$), and (3) flow in gaps that exist between stem wakes, where the flow speeds are greater than $u(z)$ [*Nepf*, 2004]. The effects of these mechanisms of velocity variation on longitudinal dispersion is quantified by [*Nepf*, 2004]

$$D_x = \sqrt{\frac{C_D^3 Re_t}{128}} ud + \frac{C_D a d^2 u}{4(1-ad)} + \gamma a d u^2 \tau \qquad (6)$$

[35] The first, second, and third terms on the right hand side of (6) represent the contributions of wakes (i.e., wake-shear dispersion), gaps, and recirculation zones, respectively, where C_D is the drag coefficient, Re_t ($=ud/\nu$) is the transport Reynolds number with ν equal to the sum of the molecular and turbulent viscosities, τ is the recirculation zone residence time, and γ quantifies recirculation zone size and is function of the stem Reynolds Number (Re_d). Under the conditions tested in our study, the last two terms of (6) can be ignored because wake-shear dispersion is much greater than dispersion arising from gaps and recirculation zones.

[36] Calculations made with (6) are in good agreement with values of D_x determined from the transition zone experiments (Table 4). Owing to changes in d and u with depth, predictions of D_x vary weakly with elevation, ranging from 0.37 cm^2 s^{-1} at $z = 11$ cm to 0.40 cm^2 s^{-1} at $z = 51$ cm. This small variation is generally consistent with the observations from the transition zone experiments for which the empirical values of D_x for the shallow and deep injections are within a factor of two and, for a particular injection, the breakthrough data can be described with uniform D_x.

[37] Further evaluation of (6) suggests that D_x should be considerably greater for the ridge experiments because the diameter of the *Cladium jamaicense* leaves that dominate the ridge-flume vegetation is more than six times greater than the stem diameter of the *Eleocharis elongata* that dominates the transition zone vegetation. Although this prediction is qualitatively consistent with our observations, values of D_x computed with (6) underestimate those determined from analysis of the ridge experiments by a factor of 20 (Table 4).

[38] This mismatch may be due, in some part, to misparameterization of equation (6). We computed C_D in equation (6) as a function of Re_d using the relationship *White* [1991] derived for cylindrical stems ($C_D = 1 + 10Re_d^{-2/3}$), yet *Cladium jamaicense*, the dominant macrophyte in the ridge flume, is composed of leaves that are V-shaped in the plane normal to their long axis. Because the distribution in the orientation of the *Cladium* leaves within the ridge flume is unknown, we are unable to provide an alternative approximation of C_D. Nevertheless, inspection of published estimates of C_D for various noncylindrical objects suggests that the sensitivity of drag coefficient to changes in stem shape is insufficient to resolve the discrepancy between theoretical and empirical values of D_x [*Lee et al.*, 2004].

[39] We hypothesize that the principal reason for the underestimation of D_x is that mechanisms in addition to those accounted for by equation (6) contributed to longitudinal dispersion in the ridge experiments. Nonidealities in plant morphology may have increased the heterogeneity of the water velocity field and enhanced longitudinal mixing. Zones of stagnant or slow moving water may exist inside the edges of the V-shaped leaves or in narrowly spaced regions where the *Cladium* leaves branch away from the stems. These sources of small-scale velocity variation, which are not represented by equation (6), may be augmented by nonuniformity in the velocity field at larger scales [*Harvey et al.*, 2005; *Nepf et al.*, 2007]. In particular, heterogeneity in vegetation frontal area may further broaden the distribution in surface water velocities and, as suggested

by *Lightbody and Nepf* [2006], generate additional longitudinal spreading that is analogous to macrodispersion observed during solute transport through geologic strata of varying hydraulic conductivity [*Sudicky*, 1986].

6.3. Vertical Dispersion

[40] Vertical dispersion of the microspheres was less than longitudinal dispersion in the transition zone and ridge experiments. This anisotropy in dispersion is consistent with published observation of solute and particle transport through wetland vegetation [*Saiers et al.*, 2003; *Lightbody and Nepf*, 2006]. In the ridge experiments, where the depth-averaged stem Reynolds Number exceeded 200, vertical mixing was probably dominated by turbulent diffusion. For model systems composed of cylindrical stems of uniform diameter, the turbulent diffusion coefficient can be expressed as [*Nepf*, 1999]

$$D_z = \beta \sqrt[3]{C_D a d} u d \tag{7}$$

where β is a scaling constant with published values for vertical diffusion ranging from 0.2 for laboratory tracer experiments to 0.7 for field tracer experiments [*Nepf*, 2004; *Lightbody and Nepf*, 2006]. Computations made with β = 0.7 are within a factor of five of our estimates of D_z from the ridge experiments (Table 4), suggesting that vertical dispersion in these experiments can be inferred, at least approximately, from knowledge of flow velocity, stem density, and stem diameter. A more accurate description of vertical dispersion in the ridge experiments will require modification of equation (7) to account for complexities associated with real vegetation that may enhance vertical dispersion, such as noncylindrical stems, nonuniformity in stem diameter, and stems and leaves with nonvertical orientations.

[41] Estimates of α from the transition zone experiments were 6 to 12 times smaller than the corresponding estimates of α from the ridge experiments (Table 3), indicating that vertical dispersion was considerably smaller in the transition zone. Although the water velocities in the transition zone and ridge experiments were similar, flow in the transition zone was laminar ($Re_d \approx 20$) owing to the comparatively small stem diameter (d) within the transition zone flume (see all-species values of d in Table 1). Under laminar flow conditions, mechanical dispersion, not turbulent diffusion, represents the principal mechanism of vertical mixing [*Nepf*, 1999; *Harvey et al.*, 2005]. This mechanical dispersion is a comparatively slow mixing process that arises from small-scale heterogeneity in vegetation morphology and resulting variations in flow resistance and tortuosity of particle transport pathways. One would expect that vertical mechanical dispersion depends on water velocity, as well as the dimensions and density of the aquatic vegetation [*Nepf*, 1999]. Although there are too few field-based observations to constrain this dependence, a published estimate of vertical dispersion of TiO_2 particles during laminar flow ($Re_d \approx 3$) through an *Eleocharis* slough is an order of magnitude lower than reported here [*Saiers et al.*, 2003]. This result and our own findings imply that vertical mixing of particulate matter within the Everglades will in general be smaller in sloughs and in transition zones between adjacent ridges and sloughs than in *Cladium*-dominated ridge environments.

6.4. Particle Filtration

[42] Filtration, in addition to advection and dispersion, influenced the fate of the particle tracers. Capture by emergent vegetation likely dominated this filtration because the particles were neither sufficiently large nor dense to be removed by sedimentation during the timescale of our experiments. We obtained a reasonable description of the breakthrough curve data by representing filtration as an irreversible, first-order kinetics process. Despite the overall model-data agreement, our best fit values of λ may, as explained in section 5.2, overestimate the filtration rates in the transition zone experiments. In light of this uncertainty, we focus the remainder of our discussion of filtration on the ridge experiments and on the relationship between these results and published findings.

[43] The best fit estimates of λ can be used to infer how the filtration process reduces particle concentrations with distance along the flow path. Provided that particle capture can be represented by a first-order rate law, particle concentrations decrease exponentially with distance and the transport distance over which filtration reduces particle concentrations by one half is

$$L_{1/2} = 0.693 \frac{u}{\lambda} \tag{8}$$

[44] Application of (8) using the depth-averaged velocity and the mean λ from the shallow and deep injections of the ridge experiments yields $L_{1/2}$ = 128 m, suggesting that the long-range transport of micrometer-sized particles within ridge environments is possible. This estimate of $L_{1/2}$ is 123 times greater than $L_{1/2}$ value for TiO_2 particle transport through an *Eleocharis* slough in Everglades National Park (ENP), where filtration arose primarily from TiO_2 particle encounters with emergent stems composed of *Eleocharis elongata* and *Eleocharis cellulosa* [*Saiers et al.*, 2003]. (*Utricularia purpurea*, a floating plant, was also present near the top of the water column, but probably played a minor role in TiO_2 particle filtration because the particles were injected near middepth and the low vertical dispersion served to concentrate the particle plume beneath the *Utricularia purpurea* layer over the 7-m-long flow path in which transport was measured.) Considering that the vegetation volume fraction (ad) of the ridge flume was more than four fold greater than volume fraction associated with the *Eleocharis* stems of the ENP site [*Saiers et al.*, 2003], the $L_{1/2}$ calculations demonstrate that the ENP macrophytes (i.e., *Eleocharis elongata and Eleocharis cellulosa*) were more effective scavengers of particles than the dominant ridge-flume macrophyte (*Cladium jamaicense*).

[45] We evaluated the effectiveness of the plant stems in scavenging particles by computing a single-stem capture efficiency (η), a dimensionless parameter that expresses the ratio of the rate that particles stick to a single stem to the rate that particle approach the stem from upstream. According to equation (1), particles are removed from a unit volume of surface water at rate λC and thus are collected by (stick to) single stem at the rate $\lambda C[(1 - ad)hd/a]$, where h is the water depth and the quantity enclosed by the

Table 5. Values of R^2 That Quantify the Goodness of Model Fit to the Particle Tracer Data for Simulations That Use Combinations of Empirical (Best Fit) Estimates and Theoretical Estimates of $u(z)$, D_x, and D_z[a]

Parameter Estimation Method	Shallow Injection	Deep Injection
Transition		
Empirical $u(z)$, D_x, D_z	0.93	0.98
Theoretical $u(z)$, D_x; empirical D_z	0.92	0.98
Ridge		
Empirical $u(z)$, D_x, D_z	0.95	0.89
Theoretical $u(z)$; empirical D_x, D_z	0.73	0.72
Theoretical D_x; empirical $u(z)$, D_z	0.93	0.82
Theoretical D_z; empirical $u(z)$, D_x	0.55	0[a]

[a]An R^2 of zero indicates that the modeled solution describes the data no better than a horizontal line through the mean concentration.

brackets is the volume of water associated with a single stem. The rate at which particles approach the stem is *uChd*, giving

$$\eta = \frac{\lambda(1 - ad)}{au} \tag{9}$$

[46] The value of η computed for the ridge flume using depth-averaged measurements of a, d, and u with the mean of λ from the shallow and deep injections equals 0.002. Hence a single stem within the ridge flume was capable of capturing 0.2% of the particles that approached its projected area from the upstream direction. This estimate is two orders of magnitude less than the η value (0.29) obtained for the *Eleocharis* stems of the ENP slough [*Saiers et al.*, 2003]. The higher capture efficiency of the *Eleocharis* stems may be due, in part, to their comparatively smaller diameter, as *Palmer et al.* [2004] showed that the probability of particle interception by a smooth cylinder isolated with a laboratory flume increased as cylinder diameter decreased. Differences in particle diameter may also have contributed to the disparity in η between the ridge flume and *Eleocharis* slough and the comparatively higher surface water velocities within the ridge flume may have led to greater shear on stationary particles and lowered the probability of successful particle adhesion following particle contact with stem surfaces. Furthermore, coatings of periphyton (a matrix of algae and heterotrophic microbes) on *Eleocharis* stems may have provided favorable conditions for particle adhesion that did not exist in the *Cladium*-dominated ridge flume.

[47] Our calculations of η and $L_{1/2}$ suggest that particle filtration rates vary substantially from place to place within the Everglades. Quantification of filtration, then, will require resolution of the spatial variation in measurable properties of the flow, particles, and vegetation and the derivation of empirical or semiempirical relationship between these properties and η [see *Palmer et al.*, 2004]. These relationships could be derived by adopting approaches employed in the development of a colloid filtration theory for water-saturated porous media [see, e.g., *Yao et al.*, 1971].

6.5. Model Prediction of Particle Transport Using Parameters Estimated From Theory

[48] We evaluated the current state of predictive capability through a series of additional transport simulations. We interpolated our measurements of a and d (Table 1) over the entire water column and used these interpolated values in equations (5), (6), and (7) to compute theoretical values of $u(z)$, D_x, and D_z, respectively. We compared modeled breakthrough curves calculated with the theoretical $u(z)$, D_x, and D_z to breakthrough curves measured in our field experiments in order to evaluate the suitability of published theory for predicting advective-dispersive particle transport within wetlands.

[49] The simulations of particle transport within the transition zone flume involved using theoretical estimates of $u(z)$ and D_x in combination with the empirical (best fit) estimates of D_z and λ. (A theory appropriate for calculating D_z for the laminar flow conditions of the transition zone experiments is unavailable.) Model calculations made with theoretical estimates of $u(z)$ and D_x closely match the experimental data. The R^2 values for these transition zone simulations exceed 0.92 and are nearly equal to those computed for model simulations that used the best fit values of $u(z)$ and D_x (Table 5).

[50] We conducted three separate simulations for particle transport in the ridge flume, first with the theoretical velocity profile, then with the theoretical D_z, and finally with the theoretical D_x. Calculations of R^2 are lower for these ridge simulations, reflecting poorer agreement between empirical and theoretical parameter estimates (Table 4). Theoretical and empirical estimates of water velocity diverge near the top of the water column of the ridge flume, leading to a 0.2 reduction in R^2 when equation (5) is used to the compute velocity profile for the model simulation. Nevertheless, this model simulation accounts for nearly 75% of the variation in the observations from both the shallow-injection and deep-injection experiments. Theoretical values of D_x are 20 fold less than corresponding empirical estimates (Table 4), yet yield model fits with $R^2 \geq 0.82$ (Table 5), suggesting that predictions of particle transport are not strongly sensitive to changes in D_x, at least for the conditions tested in our ridge experiments. Predictions of particle transport through the ridge flume are considerably more sensitive to changes in D_z. Although theoretical and best fit estimates of this parameter are within a factor of five (Table 4), R^2 values for simulations that use D_z from theory do not exceed 0.55. On the basis of this result, we infer that accurate specification of D_z is requisite to prediction of particle transport, and thus further refinement of approaches for quantifying D_z that are suitable for complex wetland environments is needed.

7. Conclusions

[51] We conclude that the advection, dispersion, and filtration of micrometer-sized particles within Everglades surface waters differ between ridge and transition zone environments that are distinguishable on the basis of flow regime and aquatic vegetation composition. This sensitivity of particle mobility to changes in flow and vegetation presents a challenge to scientists and engineers seeking to predict the transport of particles and particle-associated

chemicals (e.g., phosphorous) within the Everglades and within other wetland systems.

[52] Although our attempts to predict particle transport in the transition and ridge flumes cannot be considered a complete success, the general agreement between observed and modeled results is encouraging and suggests that a predictive framework for particle transport in wetland environments is tractable. Continued progress toward the development of this framework will rely on additional observations from the laboratory and field that can be used to evaluate models for particle transport within emergent canopies and on observations made at scales larger than considered here, where lateral heterogeneity in vegetation properties will complicate descriptions of flow and advective-dispersive transport.

[53] **Acknowledgments.** We are grateful to the thoughtful comments provided by Patricia Wiberg, Urs Neumeier, an anonymous reviewer, and Heidi Nepf (Associate Editor) that led to revisions that improved this manuscript. The authors thank L. Larsen, A. Riscassi, J. Detty, and J. O'Reilly for their participation in the field tracer experiments in the Everglades. This study was funded by the U.S. Geological Survey.

References

Ackerman, J. D. (2002), Diffusivity in a marine macrophyte canopy: Implications for submarine pollination and dispersal, *Am. J. Bot.*, *89*, 1119–1127.

Bazante, J., G. Jacobi, H. M. Solo-Gabriele, D. J. Reed, S. Mitchell-Bruker, D. L. Childers, L. A. Leonard, and M. Ross (2006), Hydrologic measurements and implications for tree island formation within Everglades National Park, *J. Hydrol.*, *329*, 606–619.

Cavalcanti, G. G., and B. G. Lockaby (2006), Effects of sediment deposition on aboveground net primary productivity, vegetation composition, and structure in riparian forests, *Wetlands*, *26*, 400–409.

Chistiansen, T., P. L. Wiberg, and T. G. Milligan (2000), Flow and sediment transport on a tidal marsh surface, *Estuarine Coastal Shelf Sci.*, *50*, 315–331.

Domenico, P. A. (1987), An analytical model for multidimensional transport of a decaying contaminant species, *J. Hydrol.*, *91*, 49–58.

Elliot, A. A. (2000), Settling of fine sediment in a channel with emergent vegetation, *J. Hydraul. Eng.*, *126*, 570–577.

Fischer, H. B., E. J. List, R. Koh, J. Imberger, and N. H. Brooks (1979), *Mixing in Inland and Coastal Waters*, 483 pp., Academic, San Diego, Calif.

Harvey, J. W., J. E. Saiers, and J. T. Newlin (2005), Solute transport and storage mechanisms in wetlands of the Everglades, south Florida, *Water Resour. Res.*, *41*, W05009, doi:10.1029/2004WR003507.

Harvey, M., E. Bourget, and R. G. Ingram (1995), Experimental evidence of passive accumulation of marine bivalve larvae on filamentous epibenthic structures, *Limnol. Oceanogr.*, *40*, 94–104.

Hosokawa, Y., and T. Horie (1992), Flow and particulate nutrient removal by wetlands with emergent macrophytes, in *Marine Coastal Eutrophication: Science of the Total Environment*, edited by R. Vollenweider, R. Marchetti, and R. Viviani, pp. 1271–1282, Elsevier, New York.

Lee, J. K., L. C. Roig, H. Jenter, and H. M. Visser (2004), Drag coefficients for modeling flow through emergent vegetation in the Florida Everglades, *Ecol. Eng.*, *22*, 237–248.

Leonard, L. A., and M. E. Luther (1995), Flow hydrodynamics in tidal marsh canopies, *Limnol. Oceanogr.*, *40*, 1474–1484.

Leonard, L. A., and D. J. Reed (2002), Hydrodynamics and sediment transport through tidal marsh canopies, *J. Coastal Res.*, *SI 36*, 459–469.

Leonard, L. A., A. C. Hine, and M. E. Luther (1995), Surficial sediment transport and deposition processes in a *Juncus roemercianus* marsh, west-central Florida, *J. Coastal Res.*, *11*, 322–336.

Lightbody, A. F., and H. M. Nepf (2006), Prediction of velocity profiles and longitudinal dispersion in emergent salt marsh vegetation, *Limnol. Oceanogr.*, *51*, 218–228.

Lodge, T. E. (2005), *The Everglades Handbook*, 302 pp., CRC Press, Boca Raton, Fla.

National Research Center (2003), Does water flow influence Everglades landscape patterns?, 41 pp., Comm. on the Restoration of the Greater Everglades Ecosyst., Washington, D.C.

Nepf, H. M. (1999), Drag, turbulence, and diffusion in flow through emergent vegetation, *Water Resour. Res.*, *35*, 479–489.

Nepf, H. M. (2004), Vegetated flow dynamics, *Ecogeomorphology of Tidal Marshes*, *Coastal Estuarine Stud.*, vol. 59, edited by S. Fagherazzi, M. Marani, and L. Blum, pp. 137–163, AGU, Washington, D.C.

Nepf, H. M., C. G. Mugnier, and R. A. Zavistoski (1997a), The effects of vegetation on longitudinal dispersion, *Estuarine Coastal Shelf Sci.*, *44*, 675–684.

Nepf, H. M., J. A. Sullivan, and R. A. Zavistoski (1997b), A model for diffusion within emergent vegetation, *Limnol. Oceanogr.*, *42*, 1735–1745.

Nepf, H., M. Ghisalberti, B. White, and E. Murphy (2007), Retention time and dispersion associated with submerged aquatic canopies, *Water Resour. Res.*, *43*, W04422, doi:10.1029/2006WR005362.

Neumeier, U., and P. Ciavolo (2004), Flow resistance and associated sedimentary processes in a *Spartina maritima* salt marsh, *J. Coastal Res.*, *20*, 435–447.

Noe, G. B., D. L. Childers, and R. D. Jones (2001), Phosphorous biogeochemistry and the impact of phosphorous enrichment: Why is the Everglades so unique?, *Ecosystems*, *4*, 603–624.

Noe, G. B., J. W. Harvey, and J. E. Saiers (2007), Characterization of suspended particles in Everglades wetlands, *Limnol. Oceanogr.*, *52*, 1166–1178.

Palmer, M. R., H. M. Nepf, and T. J. R. Pettersson (2004), Observation of particle capture on a cylindrical collector: Implications for particle accumulation and removal in aquatic systems, *Limnol. Oceanogr.*, *49*, 76–85.

Press, W. H., B. P. Flannery, S. A. Teukolsky, and W. T. Vetterling (1989), *Numerical Recipes*, 702 pp., Cambridge Univ. Press, Cambridge, U. K.

Riscassi, A. L., and R. W. Schaffranek (2003), Flow velocity, water temperature, and conductivity in Shark River Slough, Everglades National Park, Florida: August 2001–June 2002, *U.S. Geol. Surv. Open File Rep., 03–348*.

Saiers, J. E., J. W. Harvey, and S. E. Mylon (2003), Surface-water transport of suspended matter through wetland vegetation of the Florida everglades, *Geophys. Res. Lett.*, *30*(19), 1987, doi:10.1029/2003GL018132.

Sansalone, J. J., and S. G. Buchberger (1997), Characterization of solid and metal element distributions in urban highway stormwater, *Water Sci. Technol.*, *36*, 155–160.

Science Coordination Team (2003), The role of flow in the Everglades ridge and slough landscape, S. Fla. Ecosyst. Work. Group, U. S. Geol. Surv., Reston, Va. (Available at http://sofia.usgs.gov/publications/papers/sct_flows/index.html.)

Sklar, F. H., and A. van der Valk (2003), *Tree Islands of the Everglades*, Kluwer Acad., Dordrecht.

Stevenson, J., M. Kearney, and E. Pendleton (1985), Sedimentation and erosion in a Chesapeake Bay brackish marsh system, *Mar. Geol.*, *67*, 213–235.

Stumpf, R. P. (1983), The process of sedimentation on the surface of a salt marsh, *Estuarine Coastal Shelf Sci.*, *17*, 495–508.

Sudicky, E. A. (1986), A natural gradient experiment on solute transport in a sand aquifer: Spatial variability of hydraulic conductivity and its role in the dispersion process, *Water Resour. Res.*, *22*, 2069–2088.

Tritton, D. J. (1988), *Physical Fluid Dynamics*, 2nd ed., Oxford Sci., Oxford, U. K.

White, F. M. (1991), *Viscous Fluid Flow*, McGraw-Hill, New York.

Yao, K. M., M. T. Habibian, and C. R. O'Melia (1971), Water and waste water filtration: Concepts and applications, *Environ. Sci. Technol.*, *5*, 1105–1112.

J. W. Harvey and G. B. Noe, U.S. Geological Survey, 430 National Center, Reston, VA 20192, USA.

Y. H. Huang, Department of Biological and Agricultural Engineering, Texas A&M University, College Station, TX 77843, USA.

S. Mylon, Department of Chemistry, Lafayette College, Easton, PA 18042, USA.

J. E. Saiers, School of Environmental Studies, Yale University, New Haven, CT 06511, USA. (james.saiers@yale.edu)